Journal of Electronic Materials (2021) 50:6448–6458
https://doi.org/10.1007/s11664-021-09178-y

ORIGINAL RESEARCH ARTICLE

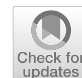

Optical and Electrical Properties of Pyrene–Imine Organic Interface Layer Based on *p*-Si

Ali Yeşildağ[1] · Musa Erdoğan[2] · Ömer Sevgili[3] · Zakir Çaldıran[4] · İkram Orak[3,5]

Received: 17 February 2021 / Accepted: 18 August 2021 / Published online: 3 September 2021
© The Minerals, Metals & Materials Society 2021

Abstract

In the present study, 1,4-phenylenebis-1-(pyren-1-yl)methanimine derivative **3** ($C_{40}H_{24}N_2$) was synthesized in high yield by condensation reaction of pyrene-1-carbaldehyde (**1**) with benzene-1,4-diamine (**2**). The structures of the obtained organic compound **3** were determined by nuclear magnetic resonance (NMR), infrared (IR), and high-resolution mass spectrometry (HRMS) spectroscopic techniques. An Al/$C_{40}H_{24}N_2$/*p*-Si device was then fabricated using this pyrene–imine-based organic material **3** at the interface. The organic layer was coated on *p*-Si by the spin coating method, and ohmic and rectifier contacts were deposited by thermal evaporation. Besides optical measurements, such as ultraviolet (UV) absorbance and NMR, the electrical and photovoltaic properties were investigated by current–voltage (*I*–*V*) measurements in the dark and under different illumination conditions and capacitance–conductance–voltage (*C*–*G*–*V*) measurements at various frequencies. The electrical parameters of the device, such as ideality factor, barrier height, and series resistance, were calculated using three methods: thermionic emission theory (TE), Cheung method, and Norde functions. Using the TE method, the ideality factor value of the six devices (D1 to D6) obtained by coating the $C_{40}H_{24}N_2$ organic layer between the metal and the semiconductor was 2.02 to 2.06, and the barrier height value increased by between 0.77 eV and 0.78 eV compared with the reference device. According to these results, the organic interface coated between the metal and semiconductor increased the barrier height and rectifying ratio of the device. In addition to its rectification feature, the Al/$C_{40}H_{24}N_2$/*p*-Si/Al device showed photodiode characteristics. Although its solar cell parameters were low, these photodiode characteristics indicate that this device could be used in optoelectronic applications.

Keywords Pyrene · imine · Schottky barrier diode · photodiode

Introduction

Organic materials are commonly used in electronic and optoelectronic devices including photodiodes,[1] thin-film transistors,[2] sensors,[3] and solar cells.[4,5] In particular, optoelectronic devices can be improved by using various materials such as organic molecules, organometallics,[6] and polymer structures.[7] Photodiodes are commonly used in photovoltaics due to their features. Many prominent researchers have investigated the performance of organic photodiodes. The performances of organic devices made from organic materials have been examined using different methods.[8–12] However, very few studies have been performed on devices made using pyrene–imine organic materials. Imine binding (–C=N–) groups are a structural motif used in ligands for metal complexes and various compounds applied as organic electronic and optoelectronic materials.[13,14] The great advantage of these structures is that they can be synthesized

✉ Musa Erdoğan
musaerdogan0@gmail.com

✉ İkram Orak
ikramorak@gmail.com

1 Department of Bioengineering, Faculty of Engineering and Architecture, Kafkas University, 36100 Kars, Turkey

2 Department of Food Engineering, Faculty of Engineering and Architecture, Kafkas University, 36100 Kars, Turkey

3 Vocational School of Health Services, Bingol University, 12000 Bingol, Turkey

4 Department of Electric and Energy, Ardahan Technical Science V.H.S., Ardahan University, 75000 Ardahan, Turkey

5 Renewable Energy Systems, Institute of Science, Bingol University, 12000 Bingol, Turkey

simply in a one-step condensation reaction between aldehydes and amines.[15] Moreover, they are also known to be environmentally friendly compounds, because water is the only byproduct in these reactions and complex purification is not required.[16] Because of their simplicity of preparation, these structures are significant organic semiconductors and represent alternatives to conventional conjugated compounds as they are isoelectronic with vinyl analogs.[17] On the other hand, pyrene, which has the structure of a polycyclic aromatic hydrocarbon, has attracted attention from researchers in the materials and photochemical scientific fields due to its unique fluorescence properties.[18] Pyrene can also be used as a chemical sensor for the detection of chemicals such as organic molecules as well as anionic and cationic analytes.[19]

In the work presented herein, a novel isomeric mixture of pyrene–imine-based organic material **3** was synthesized and characterized. Moreover, the photovoltaic and electrical characteristics of an Al/$C_{40}H_{24}N_2$/*p*-Si device are also reported. The electrical and photovoltaic properties were investigated using current–voltage (*I*–*V*) measurements in the dark and under different illumination conditions and capacitance–conductance–voltage (*C*–*G*–*V*) measurements at various frequencies. The electrical parameters of device D2 were calculated using the following three methods: thermionic emission (TE) theory, Cheung method, and Norde function.

Experimental Procedures

General

All commercially available chemicals were obtained from Sigma-Aldrich and used without further purification. ^{1}H nuclear magnetic resonance (NMR) spectra were recorded on a Bruker Ultrashield Plus Biospin spectrometer at 400 MHz. NMR chemical shifts were determined relative to internal standard tetramethylsilane (TMS) at δ 0.0 ppm. Chemical shifts (δ) are reported in ppm, and coupling constants (*J*) in Hertz (Hz). Melting points (M.p.) were recorded on a Stuart melting point SMP30 device and are uncorrected. Fourier-transform infrared (FTIR) spectra were recorded using a PerkinElmer Frontier FT-IR spectrophotometer. Mass spectra were recorded on an Agilent Technologies 6530 Accurate-Mass Q-TOF-LC/MS.

Synthesis of Organic Compound 3

To a 100-mL one-necked round-bottomed flask equipped with a condenser were added benzene-1,4-diamine (**2**) (0.25 g, 2.31 mmol) and ethanol (50 mL). To the above solution was added aryl pyrene-1-carbaldehyde (4.85 mmol, 1.12 g, 2.1 equiv), and the reaction mixture was refluxed for 15 h and monitored by thin-layer chromatography (TLC). After complete consumption of pyrene aldehyde **1**, the reaction mixture was concentrated under reduced pressure. The mixture was then cooled to room temperature. Upon cooling the resulting reaction solution to ambient temperature, yellow crystals precipitated from solution; the solid product was filtered and washed with cold methanol, then dried in vacuo to give isomeric mixtures **3a**,**b**. (1*E*(*Z*),1'*E*(*Z*))-*N*,*N*'-(1,4-phenylene)bis(1-(pyren-1-yl)methanimine) (***3a***,***b***): (813 mg, 95%) as yellow crystals. M.p.: 315–317 °C. ^{1}H NMR (400 MHz, $CDCl_3$): The NMR spectrum revealed that a mixture of *EE* and *ZZ* isomers of **3a**,**b** formed in the reaction. $\delta = 9.61$ (s), (*ZZ*); 9.54 (s), (*EE*). The two isomeric mixtures were formed in a 2:3 *ZZ* to *EE* ratio. IR (cm^{-1}): 3049, 3023, 3004, 1922, 1792, 1678, 1607, 1598, 1538, 1504, 1413, 1385, 1362, 1322, 1310, 1243, 1234, 1215, 1204, 1183,1139, 1105, 1053, 1007, 967, 901, 858, 848, 839, 819, 800,764, 714, 681, 613, 605. HRMS (Q-TOF): *m*/*z* $[M+H]^+$ calcd. For $C_{40}H_{25}N_2$: 533.2017, found: 533.2017.

Device Fabrication

First, a *p*-Si (100) wafer was one-side polished to thickness of 525 μm. Its resistivity was 1 ohm-cm to 10 ohm-cm. Firstly, the wafer was cut into pieces of 2.0 cm $\times$ 2.0 cm for ohmic contact. Secondly, they were chemically cleaned using standard procedures; the pieces were cleaned using acetone for 600 s by ultrasonic vibration, then rinsed with DI water. The pieces were cleaned using isopropanol alcohol for 600 s by ultrasonic vibration, then rinsed with DI water. For the final cleaning step, the pieces were subjected to diluted HF for 30 s, then rinsed by ultrasonic vibration in DI water and dried using N_2. Al was deposited by thermal evaporation. The *p*-Si/Al structure was annealed at 450 °C for 5 min in N_2 atmosphere for ohmic contact with rapid thermal annealing (RTA). Stock solutions of $C_{40}H_{24}N_2$ (10^{-3} mol L^{-1}) were prepared in dimethyl sulfoxide (DMSO). $C_{40}H_{24}N_2$ was directly formed by adding 2 μL 0.001 M $C_{40}H_{24}N_2$ in DMSO on the front surface of the *p*-Si substrate. The organic solution was then spin-coated onto the Si substrates by rotating at 1000 rpm/min for 30 s. The morphology of the interface layer sandwiched between the metal and semiconductor affects the electrical properties of the structure. A SEM image of the pyrene–imine organic layer coated on the Si surface is shown in Fig. 1a. As seen in the figure, the organic material is neatly coated on the surface of the semiconductor layer, although there are borders and cracks between regions. In this case, various electrical parameters such as the ideality factor, which indicates the quality of the structure, as well as the the surface states and barrier height of the diode are affected. Additionally, the thickness of the interface layer used affects the electrical properties of the structure.[20,21] Reddy et al.[21] examined the

surface morphology and optical and electrical properties of Au/CuPc/*n*-Si heterojunctions with different thickness interface. They showed that the electrical properties of the Schottky structure can be altered by controlling the thickness of the interlayer.

The rectifier contacts were obtained by coating Al on the $C_{40}H_{24}N_2$/*p*-Si layer surface. The energy band diagram of the metal–semiconductor contact obtained with the pyrene–imine interface is shown in Fig. 1b. Carriers passing from the semiconductor to metal in thermal equilibrium will encounter a barrier known as the Schottky barrier.[22] Using a circular mask, Al metal was coated on the front surface of $C_{40}H_{24}N_2$/*p*-Si by thermal evaporation, so six different Al/$C_{40}H_{24}N_2$/*p*-Si/Al rectifier contact structures with the same conditions and similar properties were obtained. This is a metalorganic–polymer–semiconductor (MPS) device. In addition, a reference Al/*p*-Si/Al metal–semiconductor device structure was obtained using the same fabrication conditions but without $C_{40}H_{24}N_2$ interface material. *I–V* measurements were carried out on all the devices in the dark at room temperature. In addition, *I–V* measurements of the Al/$C_{40}H_{24}N_2$/*p*-Si/Al device with the best device parameters were carried out under different illumination values using a solar simulator and *C–V* measurements were carried out at different frequency values. A schematic diagram of the Al/$C_{40}H_{24}N_2$/*p*-Si/Al structure and electrical measurement system is shown in Fig. 2.

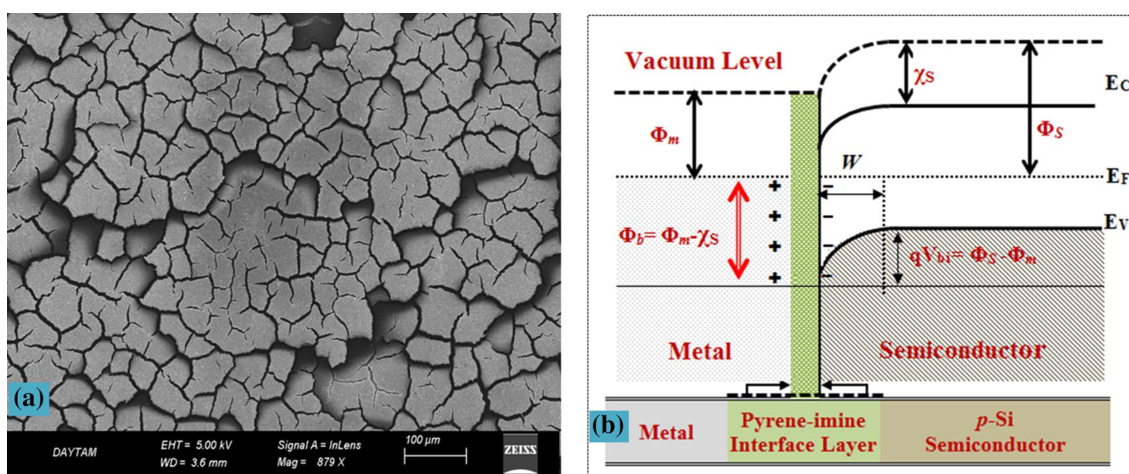

Fig. 1 SEM image of $C_{40}H_{24}N_2$ organic layer (a) and schematic of energy band diagram for Al/$C_{40}H_{24}N_2$/*p*-Si rectifier contact (b).

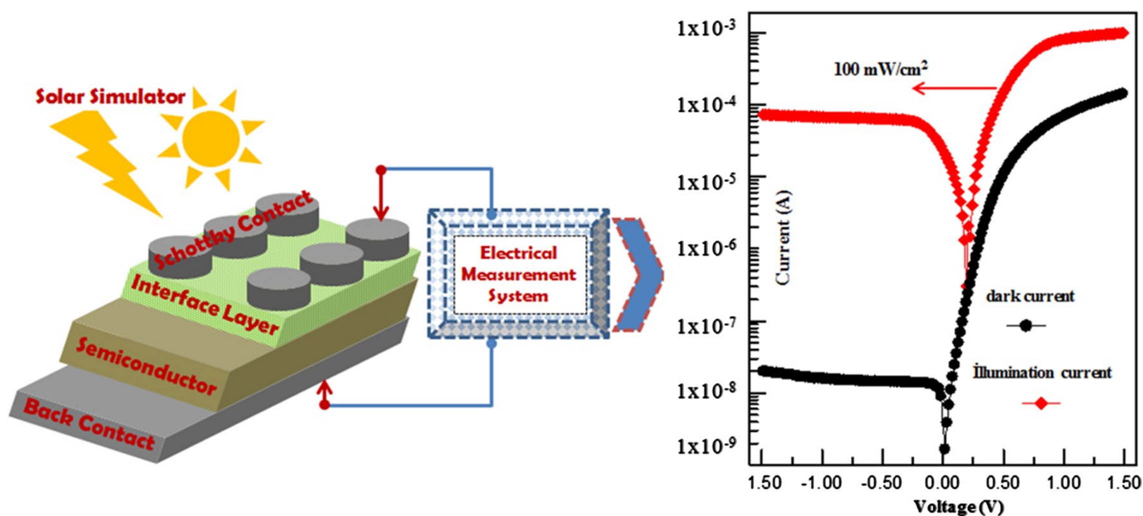

Fig. 2 Schematic diagram of Al/$C_{40}H_{24}N_2$/*p*-Si/Al structure and electrical measurement system.

Results and Discussion

Synthesis

Pyrene-1-carbaldehyde (**1**), which was commercially available, became the key structure that allowed us to prepare the organic material **3**. A schematic representation of the synthesized organic compound is shown in Fig. 3. Compound **3** was synthesized via one-pot condensation of pyrene-1-carbaldehyde (**1**) and benzene-1,4-diamine (**2**) in ethanol with excellent yield (95%) (lit.,[17] yield 19%). The ^{1}H NMR spectrum revealed that a mixture of *EE* and *ZZ* isomers was formed in the reaction.

The ^{1}H NMR spectrum of the isomers **3a**,**b**, which has a symmetrical structure, consists of sets of signals appearing in the aromatic region (Fig. 4). The characteristic imine (C=N) protons resonate as a singlet at 9.61 ppm for *ZZ* isomer **3a** and at 9.54 ppm for *EE* isomer **3b**. The two isomeric mixtures were formed in a 2:3 *ZZ* to *EE* ratio.

High-resolution mass spectrometry (HRMS) confirmed the constitution of the isomers **3a**,**b**. The HRMS results showed excellent agreement between the calculated (533.2017) and obtained mass (533.2017), with both values turning out to be exactly the same (Fig. 5). Since the molecular formulas of isomers **3a**,**b** are the same, their calculated masses are also the same.

The IR spectrum of compound **3** exhibited characteristic absorption bands at about 3049 cm^{-1} and 1385 cm^{-1}. The C–H stretching band was seen at 3049 cm^{-1}. The C–C stretching band was also seen at 1385 cm^{-1}. Moreover, the IR spectra of compound **3** showed one characteristic band at 1607 cm^{-1}, indicating formation of the imine (C=N) group (Fig. 6).

Figure 7a shows the ultraviolet–visible (UV–Vis9 absorption spectra of the synthesized compound **3** in DMSO as solvent. The absorption spectrum of compound **3** shows two distinct bands at 292 nm and 432 nm, which may derive from the *n*–π*/π–π* transitions on pyrene, benzene, and imine cores in the structure of compound **3**. Considering the maximum absorbance peak at 432 nm, the energy bandgap of compound **3** was calculated from Fig. 7b using the Tauc method[23] to be 2.49 eV.

Current–Voltage Characteristics of Al/$C_{40}H_{24}N_2$/*p*-Si Device

To understand the effects of the material used as an interfacial layer, the electrical properties, such as the current–voltage (*I*–*V*) and capacitance–voltage (*C*–*V*) characteristics, of the fabricated devices should be examined. The *I*–*V* characteristics of the Al/$C_{40}H_{24}N_2$/*p*-Si/Al device were measured in the dark and junder illumination. In addition, *I*–*V* measurements were carried out on the Al/*p*-Si/Al reference device at room temperature and in the dark. The device showed rectifying behavior under all conditions. For devices, the leakage current was observed at reverse bias, while the current at low voltage was saturated under forward bias.[23] Accordingly, this device is suitable for electronic and photovoltaic applications at room temperature. The basic electrical diode parameters of the device were calculated from the *I*–*V* measurements using thermionic emission (TE) theory:[24]

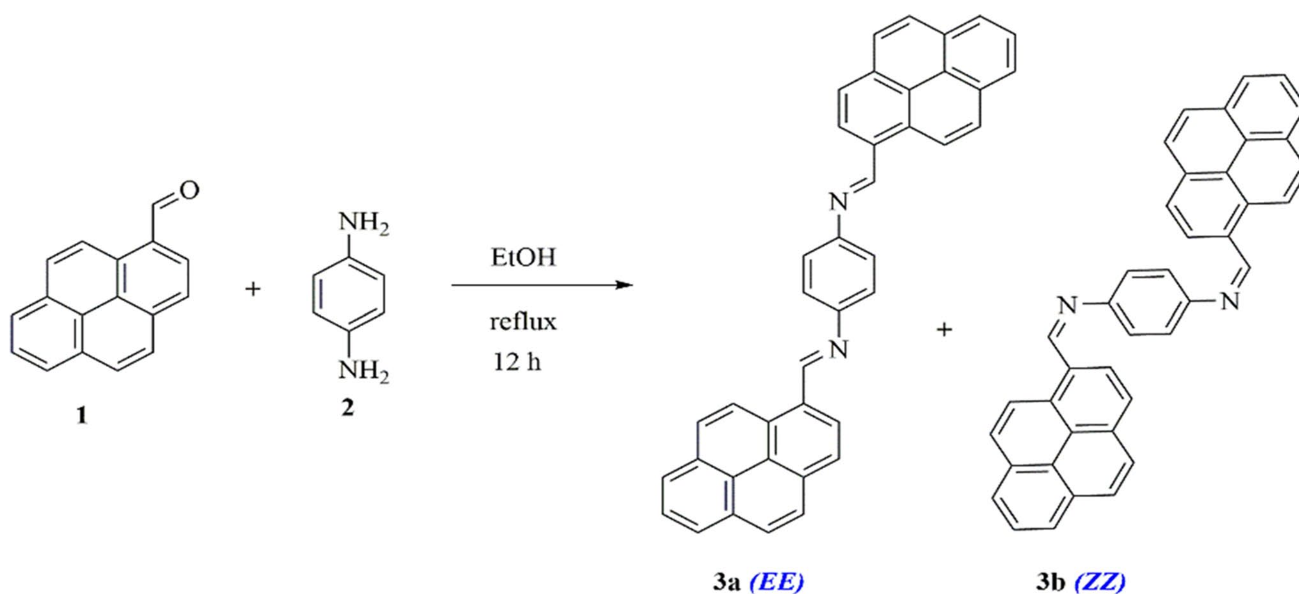

Fig. 3 Synthesis of isomers **3a**,**b**.

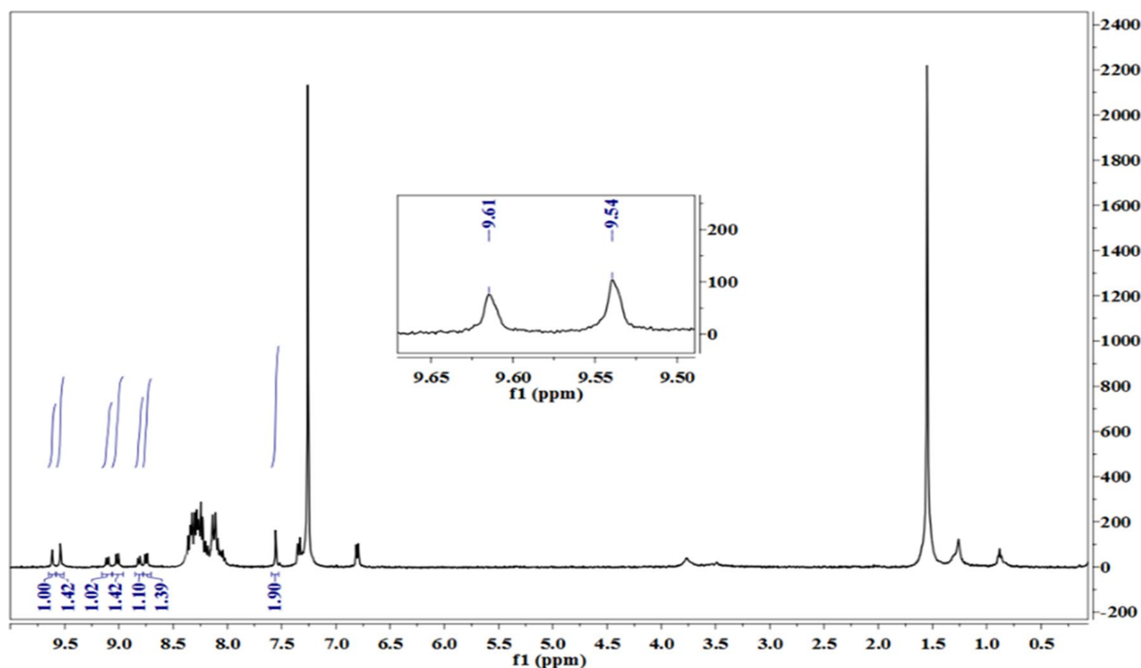

Fig. 4 ^{1}H NMR (400 MHz, $CDCl_3$) spectrum of isomers **3a**,**b**.

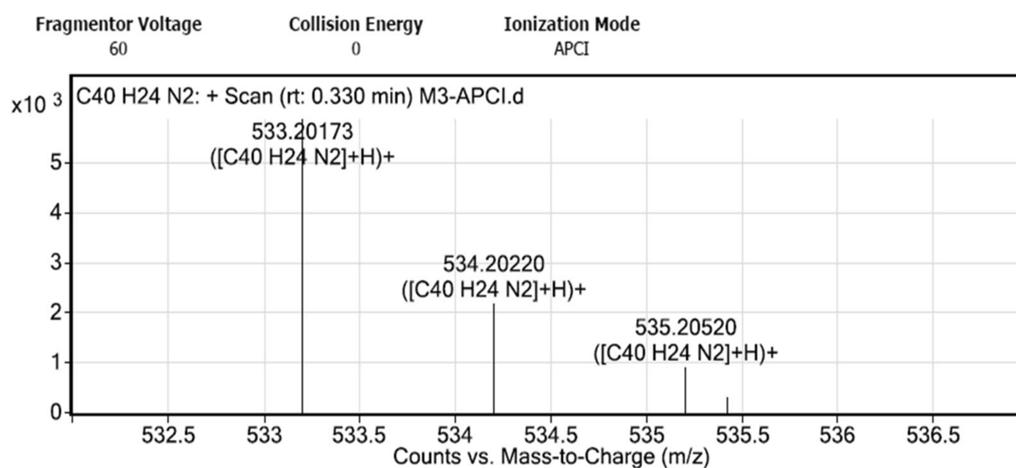

Fig. 5 HRMS spectrum of isomers **3a**,**b**.

$$I = I_0\left[\exp\left(-\frac{q(V - IR_s)}{kT}\right) - 1\right], \tag{1}$$

where I_0 is the leakage current found as the intercept of the linear part of the ln I–V graph when the voltage value was zero as follows:[25]

$$I_0 = AA^*T^2\exp\left(-\frac{q\Phi_b}{kT}\right), \tag{2}$$

where A, A^*, T, q, Φ_b, and k terms stand for the effective diode area, Richardson constant, zero-bias temperature, electronic charge, barrier height, and Boltzmann constant, respectively. The experimental n and Φ_b values can be obtained from Eqs. 3 and 4:[26]

$$n = \frac{q}{kT}\left(\frac{dV}{d(\ln I)}\right), \tag{3}$$

and

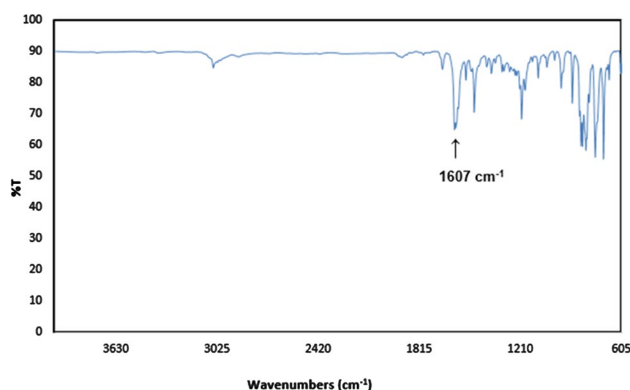

Fig. 6 IR spectrum of isomers **3a**,**b**.

$$\Phi_b = \frac{kT}{q}\ln\left(\frac{AA^*T^2}{I_0}\right). \tag{4}$$

Figure 8a shows the *I–V* characteristics of the Al/$C_{40}H_{24}N_2$/*p*-Si/Al and Al/*p*-Si/Al devices at room temperature in dark condition. The ideality factor of the device obtained without the $C_{40}H_{24}N_2$ organic material was calculated to be 1.90 with a barrier height of 0.66 eV. On the other hand, the ideality factor value of the six devices (D1 to D6) obtained by coating a $C_{40}H_{24}N_2$ organic layer between the metal and semiconductor varied between 2.02 and 2.06 with barrier height values between 0.77 eV and 0.78 eV. As seen from Fig. 8a, coating a thin organic layer between the metal and semiconductor allowed the current to increase more linearly at low voltages. On the other hand, the interfacial layer prevented leakage current and reduced the reverse-bias current.[22,23] According to these results, the organic interface coated between the metal and semiconductor increased the barrier height of the devices.[27,28] This change can be seen in Fig. 8b. A high ideality factor value is available in literature;[29–33] For example; Ongun et al.[29] fabricated Au/BOD-Pyr/*n*-Si/In Schottky diode and found an ideality factor value of 2.4 and 8.7 for two different regions in the dark, respectively. In the same study, they found the barrier height to be 0.75 eV and 0.71 eV for two different regions, respectively. The rectification ratio of the Al/$C_{40}H_{24}N_2$/*p*-Si/Al device obtained with the $C_{40}H_{24}N_2$ organic interface was greater than that of the reference device.[22]

Figure 9a shows the logarithmic *I–V* measurements of Al/$C_{40}H_{24}N_2$/*p*-Si/Al device (D2) carried out at room temperature and under different illuminations values of 30 mW/cm^2, 40 mW/cm^2, 60 mW/cm^2, 80 mW/cm^2, and 100 mW/cm^2. The electrical characteristics of the device reveal ideal Schottky diode behavior and rectification. According to TE theory, n and Φ_b were calculated to be 2.04 eV and 0.78 eV using Eq. 3 and 4, respectively. In an ideal diode for electrical and electronic applications, n should be 1, but it is usually greater than 1 due to imperfections, such as tunneling current, interface state, inhomogeneity, deposition condition, and series resistance effect.[34–36] In addition to the *I–V* measurements in the dark, the photovoltaic performance of the device was investigated under illumination conditions. The reason for taking such measurements is to examine the response of the device under different light intensities. As seen in Fig. 9a, as the light intensity was gradually increased, the photocurrent values also increased. Figure 9b shows the linear *I–V* graph of the Al/$C_{40}H_{24}N_2$/*p*-Si/

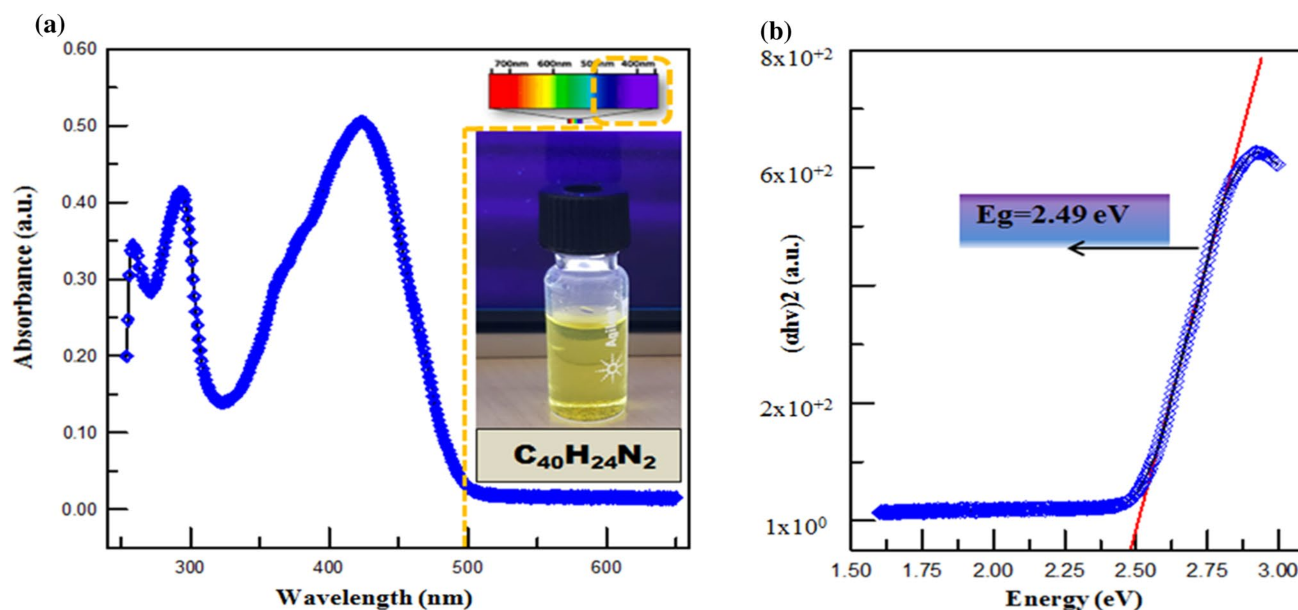

Fig. 7 UV–Vis absorption spectra of $C_{40}H_{24}N_2$ organic thin film (a). Inset: plot of $(\alpha h\nu)^2$ versus ($h\nu$) (b).

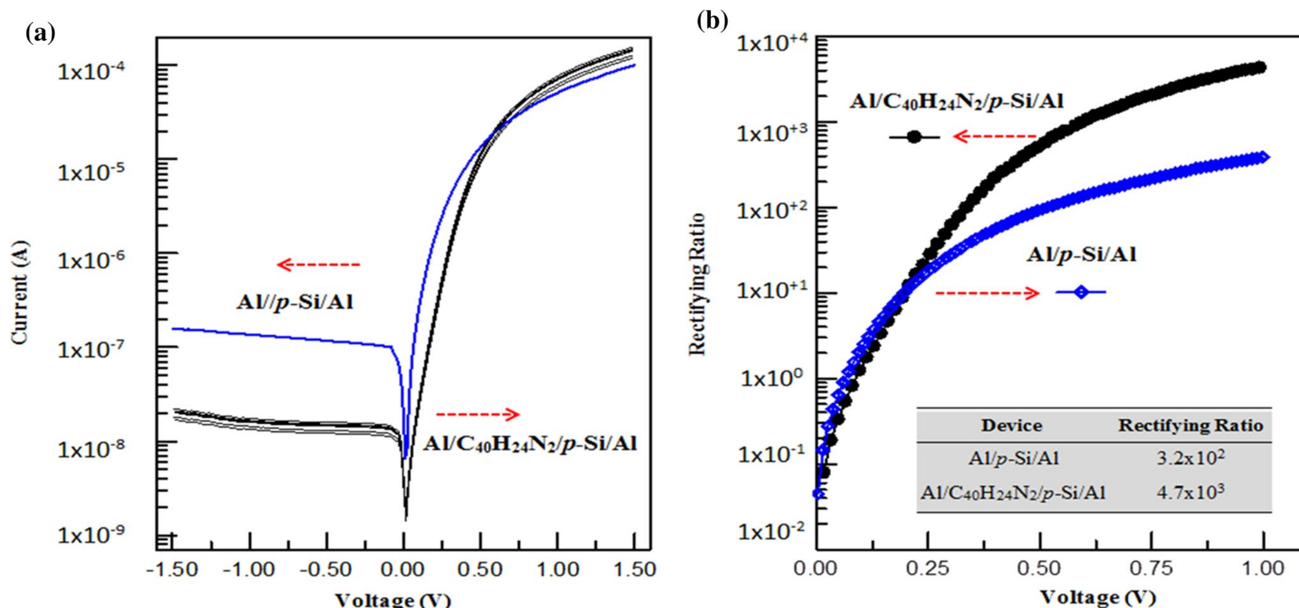

Fig. 8 *I–V* characteristics of different devices at room temperature in the dark (a) and rectifying ratio–voltage plots for reference diode and Al/$C_{40}H_{24}N_2$/*p*-Si/Al diode (b).

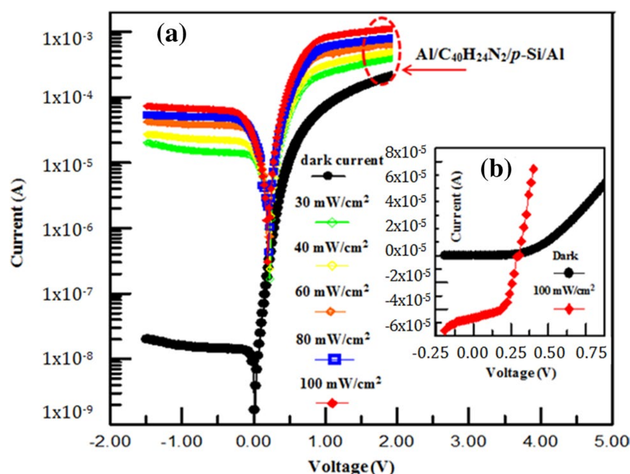

Fig. 9 Logarithmic *I–V* characteristics of the device in the dark and under different illumination values (a) and linear *I–V* characteristics of the device in the dark and under 100 mW/cm^2 (b).

Al device int he dark and under 100 mW/cm^2 illumination. It is clear from this graph that the reverse-bias current of the device increased under illumination. This is a desirable physical property. Because the device is based on *p*-Si, the conversion efficiency is very low for solar cell applications. Thus, the device behaved like a photodiode under illumination. Yıldız et al.[30] examined the electrical properties of Au/4H-SiC Schottky diode under illumination. They showed that, with increasing illumination intensity, the barrier height increased while the ideality factor decreased.

Based on these electrical characterization results, the Cheung and Norde function methods were used to determine the value of various diode parameters, such as the series resistance (R_s), n, and Φ_b of the Al/$C_{40}H_{24}N_2$/*p*-Si/Al device D2. These diode parameters can be checked and compared using different methods. The Cheung method is applied in the region where the *I–V* graphs in Fig. 10 move away from linearity in the forward-bias region. The series resistance and barrier height values can be obtained according to Cheung's function:[37,38]

$$H(I) = V - n\left(\frac{kT}{q}\right)\ln\left(\frac{I}{AA^*T^2}\right) = n\Phi_b + IR_s, \quad (5)$$

$$\frac{dV}{d(\ln I)} = \frac{nkT}{e} + IR_s. \quad (6)$$

R_s values were found from the slope of the $H(I)$–I plots and dV/d(ln$I$)–I in Fig. 10. The values of n and Φ_b were calculated from the points where the dV/d(ln$I$)–I and $H(I)$–I plots intersected the vertical axis, respectively. The Cheung functions used and the calculated diode parameters are presented in Table I. In Fig. 10a, the plot of $H(I)$ versus I is linear, and the slope of this plot gives the R_s value of the device, while the intercept gives the n and Φ_b values. The n value is given in Eq. 3. Thus, the Φ_b and R_s values can be calculated. Accordingly, dV/d(ln$I$) versus I with respect to Eq. 6 also gives a straight line. The slope and y-intercept of this plot are equal to R_s and nkT/q. The n values can be calculated from the intercept of the plot. Two different R_s values

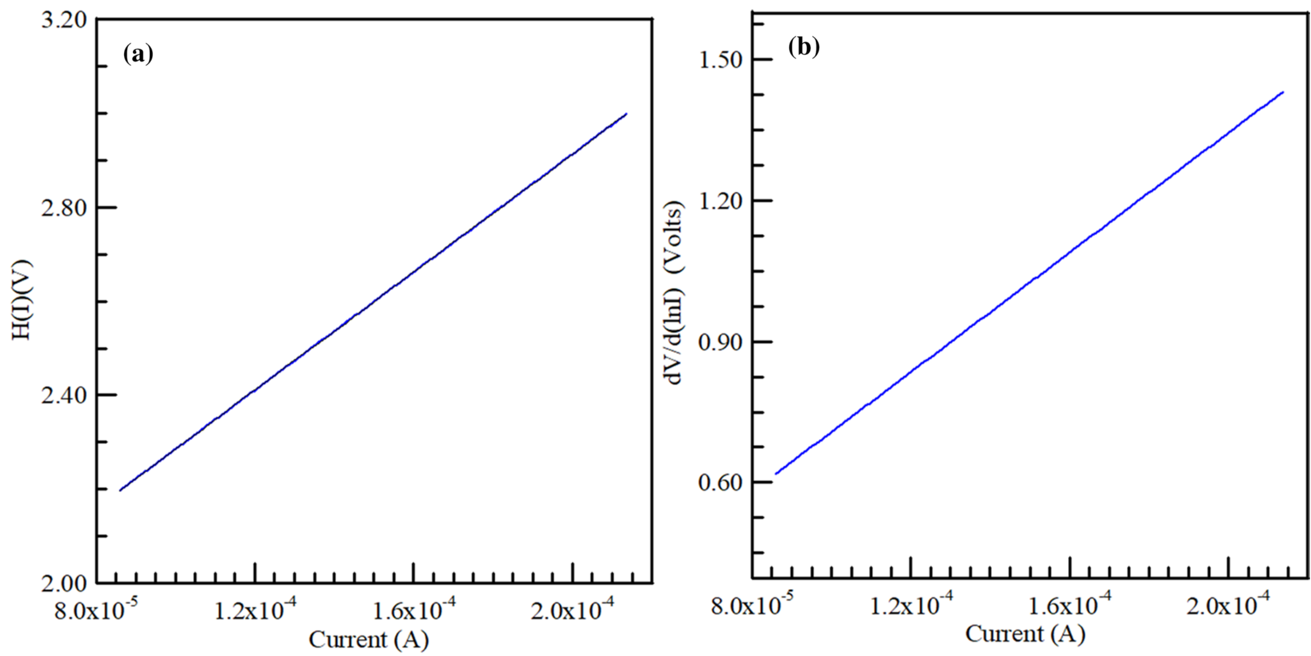

Fig. 10 (a) $H(I)$ versus I and (b) $dV/d(\ln I)$ versus I plots of device.

Table I Diode parameters of $Al/C_{40}H_{24}N_2/p$-Si/Al device D2 calculated from I–V measurements

n TE	n Cheung	Φ_b (eV) TE	Φ_b (eV) Cheung	Φ_b (eV) Norde	R_s (kΩ) Cheung-$H(I)$	R_s (kΩ) Cheung-$d\ln(I)$	R_s (kΩ) Norde
2.04	2.75	0.77	0.82	0.79	6.23	6.36	0.67

are obtained from different fit data according to the Cheung approximation. According to the $H(I)$–I plot, R_s and Φ_b values of 6.23 kΩ and 0.82 eV, respectively, were calculated. Using the $dV/d(\ln I)$–I plot, R_s and Φ_b values of 6.36 kΩ and 2.75, respectively, were obtained. The main reason for the different results obtained from I–V calculations using the TE and Cheung methods is that they use different regions of the graph.[39] In addition, different Φ_b and n values are calculated due to the R_s effect and the change of the interface states.[37,40]

Furthermore, Norde proposed another method to determine R_s and Φ_b values, as follows:[25,35,38]

$$F(V) = \frac{V}{\gamma} - \frac{kT}{q}\ln\left(\frac{I(V)}{AA^*T^2}\right), \quad (7)$$

$$\Phi_b = F(V_{min}) + \frac{V_{min}}{\gamma} - \frac{kT}{q}, \quad (8)$$

$$R_s = \frac{kT(\gamma - n)}{qI_{min}}. \quad (9)$$

In these formulas, $F(V_{min})$ is the minimum value of the F–V curve, the minimum current corresponding to I_{min}, $F(V_{min})$ is the minimum applied voltage corresponding to V_{min} $F(V_{min})$, where γ is an arbitrary integer greater than n ($\gamma > n$); here $\gamma = 3$ is used. $F(V)$–V plots for the devices are shown in Fig. 11. From these graphs, the minimum values for I, V, F were determined, and the values of Φ_b and R_s calculated using Eqs. 8 and 9 are presented in Table I. The Φ_b and R_s values of the structure were calculated to be 0.79 eV and 672 Ω, respectively, using $F(V_0) = 0.75$ V and $V_0 = 0.19$ V. It is understood from literature that the

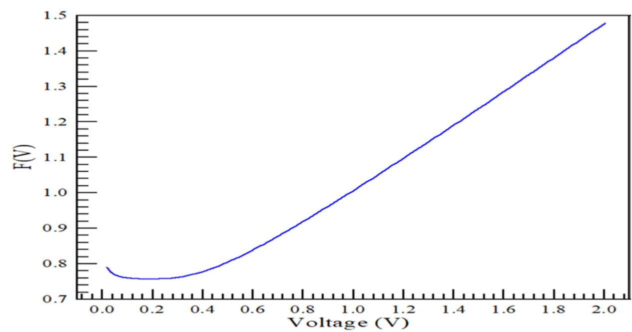

Fig. 11 $F(V)$–V plot of device.

interface material and the metal contacts used change the basic electrical parameters such as n, Φ_b, and R_s.[41]

Capacitance–Voltage and Conductance–Voltage Characteristics of the Device

The other electrical characteristics of the device are the capacitance–voltage (C–V) and conductance–voltage (G–V) measurements. The C–V and G–V plots are shown in Fig. 12a and b, respectively. The C–V and G–V measurements were taken at different frequencies such as 1 kHz, 10 kHz, 100 kHz, and 1000 kHz. In Fig. 12a, the C values increase with increasing voltage but decrease with increasing frequency. The reason for these behaviors depends on the series resistance and interface states.[42,43] In Fig 12b, the G measurement was carried out at the same frequencies. The G values increased with increasing voltage, but the conductance increased with increasing frequency, in contrast to the capacitance. The G values of the device did not change anywhere at low frequency. This conductance behavior can be attributed to interface states.[44,45] Furthermore, the C^{-2}–V plots was drawn from the capacitance measurements; some the main parameters, such as the Fermi energy (E_F), donor concentration (N_d), maximum electric field (E_m), and Φ_b, were calculated using the C^{-2}–V data. Figure 13 shows the reverse-bias $1/C^2$ versus V characteristics for Al/$C_{40}H_{24}N_2$/p-Si/Al device D2 (Table II).

The depletion capacitance value is given as

$$\frac{1}{C^2} = \left(\frac{2}{\varepsilon_0 q N_d A^2}\right)\left(V_{bi} - V\right), \quad (10)$$

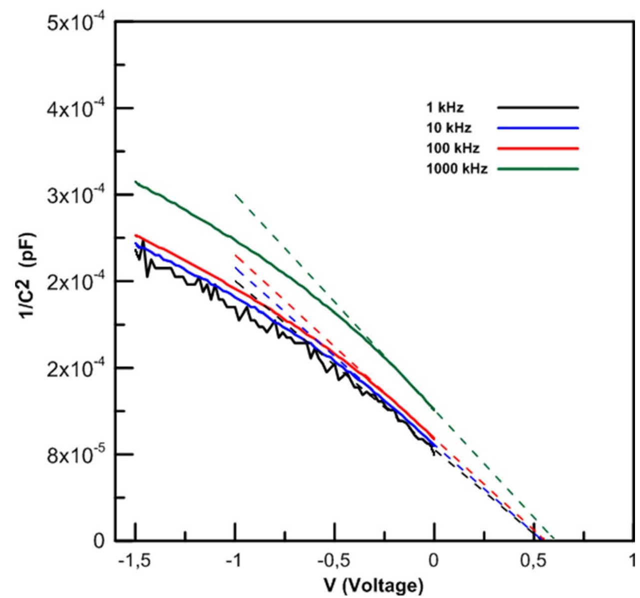

Fig. 13 Reverse-bias $1/C^2$ versus V characteristics for the device.

where V_{bi} is the built-in potential, N_d is the donor concentration, and ε_0 is the permittivity of the semiconductor. According to Schottky diode research,[46] there are two methods for barrier height calculations. The first is based on an ideal diode, while the other uses a nonideal diode.

$$\varnothing_b = V_{bi} + E_f. \quad (11)$$

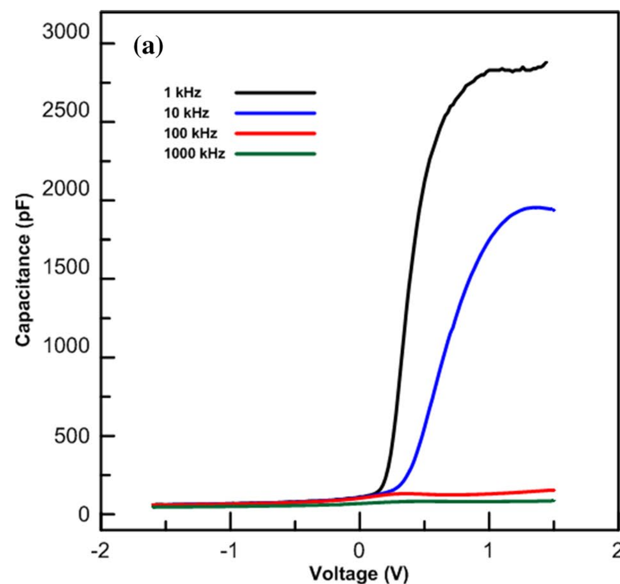

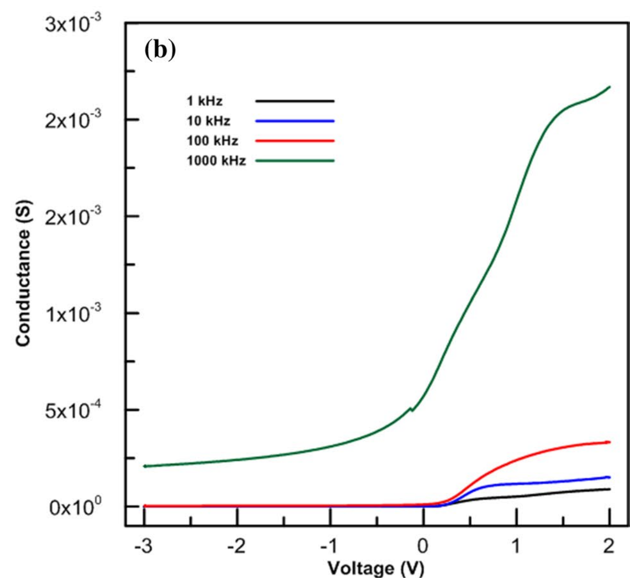

Fig. 12 Forward- and reverse-bias capacitance versus voltage (a) and conductance versus voltage (b) characteristics for the device.

Table II Electrical parameters of device at various frequencies

Frequency (kHz)	d*C*/d*V*	V_d (eV)	E_f (eV)	Φ_1	Φ_2	N_d (cm^{-3})
1	1.56×10^{-4}	0.53	0.26	0.79	0.61	1.2×10^{15}
10	1.63×10^{-4}	0.54	0.26	0.81	0.63	1.2×10^{15}
100	1.60×10^{-4}	0.58	0.26	0.84	0.69	1.2×10^{15}
1000	1.99×10^{-4}	0.61	0.27	0.87	0.71	9.8×10^{14}

If the diode is an ideal structure, the barrier height is calculated from Eq. 11. In this situation, *n* is added to the Φ_b calculations.

$$E_f = \frac{kT}{q} ln\left(\frac{N_d}{N_c}\right). \tag{12}$$

In addition, the Fermi level of the device can be calculated using Eq. 12. N_c is the density of states at the conductivity band edge. The value of N_c is 2.8×10^{19} cm^{-3} for *n*-Si at 300 K. According to the literature, some electrical parameters of the diode may vary with frequency.[47]

Conclusions

A novel isomeric mixture of efficient organic materials derived from the pyrene carboxaldehyde with benzene-1,4-diamine hybrid nucleus was synthesized and characterized. The organic material was synthesized in excellent yield using a one-pot, one-step condensation reaction and characterized using various spectroscopic techniques. To understand the electrical and optical properties of this organic material, an organic photodiode based on *p*-Si was fabricated with spin coating and thermal evaporation techniques. The photovoltaic and electrical properties of the device were investigated using different calculation approaches such as TE theory, Norde functions, and the Cheung method. *n* and Φ_b were calculated to be 2.04 and 0.78, respectively. According to the experimental results, the organic interface coated between the metal and semiconductor increased the barrier height and rectifying ratio of the device. The device showed typical rectifying behavior and photodiode characteristics at room temperature. According to these results, such devices could be used for photodiode and some diode applications due to their electrical properties. However, they are not appropriate for solar cell applications due to the low conversion efficiency. Moreover, to understand the effects of the interface layer on the capacitance and conductance characteristics, *C*–*V*–*f* and *G*–*V*–f measurements were carried out on the diode at 300 K. The performance of the device was examined by calculating different electrical parameters as a function of frequency. The results of this work highlight the consideration of using such an organic interface layer in organic photodiode applications.

Conflict of Interest On behalf of all authors, the corresponding author states that there are no conflicts of interest.

References

1. A. Pierre, I. Deckman, P.B. Lechêne, and A.C. Arias, *Adv. Mater.* 27, 6411 (2015).
2. C. Reese, M. Roberts, M.M. Ling, and Z. Bao, *Mater. Today* 7, 20 (2004).
3. D. Elkington, N. Cooling, W. Belcher, P.C. Dastoor, and X. Zhou, *Electronics* 3, 234 (2014).
4. O. Sahin, S. Kutluay, S. Horoz, and M.S. Ece, *Environ. Sci. Pollut. Res.* 28, 5231 (2021).
5. M. Erdogan, and S. Horoz, *J. Chem. Res.* 45, 207 (2021).
6. A. Yesildag, *Chem. Pap.* 75, 4949 (2021).
7. Y. Zhou, C. Fuentes-Hernandez, J. Shim, J. Meyer, A.J. Giordano, H. Li, P. Winget, T. Papadopoulos, H. Cheun, J. Kim, M. Fenoll, A. Dindar, W. Haske, E. Najafabadi, T.M. Khan, H. Sojoudi, S. Barlow, S. Graham, J.L. Brédas, S.R. Marder, A. Kahn, and B. Kippelen, *Science* 336, 327 (2012).
8. I.H. Campbell, and B.K. Crone, *Appl. Phys. Lett.* 101, 023301 (2012).
9. F. Yakuphanoglu, *Synth. Met.* 157, 859 (2007).
10. S. Tedde, E.S. Zaus, J. Fürst, D. Henseler, and P. Lugli, *IEEE Electron Device Lett.* 28, 893 (2007).
11. J. Yamaura, Y. Muraoka, T. Yamauchi, T. Muramatsu, and Z. Hiroi, *Appl. Phys. Lett.* 83, 2097 (2003).
12. J. Lee, D.K. Hwang, C.H. Park, S.S. Kim, and S. Im, *Thin Solid Films* 451, 12 (2004).
13. E. Gal, L. Găină, C. Cristea, V. Munteanu, and L. Silaghi-Dumitrescu, *J. Electroanal. Chem.* 770, 14 (2016).
14. M. Koole, R. Frisenda, M.L. Petrus, M.L. Perrin, H.S.J. Van Der Zant, and T.J. Dingemans, *Org. Electron.* 34, 38 (2016).
15. Y. Xin, and J. Yuan, *Polym. Chem.* 3, 3045 (2012).
16. M.L. Petrus, R.K.M. Bouwer, U. Lafont, S. Athanasopoulos, N.C. Greenham, and T.J. Dingemans, *J. Mater. Chem. A* 2, 9474 (2014).
17. D. Sęk, M. Siwy, J.G. Małecki, S. Kotowicz, S. Golba, E.M. Nowak, J. Sanetra, and E. Schab-Balcerzak, *Spectrochim. Acta A Mol. Biomol Spectrosc.* 175, 168 (2017).
18. J.S.S. De Melo, T. Costa, C.S. De Castro, and A.L. Maçanita, *Photochemistry* 41, 58 (2013).
19. D. Pinheiro, C.S. De Castro, J.S. Seixas De Melo, E. Oliveira, C. Nuñez, A. Fernández-Lodeiro, J.L. Capelo, and C. Lodeiro, *Dyes Pigm.* 110, 152 (2014).
20. M.D. Kaya, B.C. Sertel, N.A. Sonmez, M. Cakmak, and S. Ozcelik, *Appl. Phys. A* 126, 830 (2020).
21. P.R.S. Reddy, V. Janardhanam, I. Jyothi, C.S. Harsha, V.R. Reddy, S. Lee, J. Won, and C. Choi, *Appl. Phys. A* 124, 115 (2018).
22. Z. Caldiran, *J. Alloys Compd.* 865, 158856 (2021).
23. Z. Orhan, E. Cinan, Z. Caldıran, Y. Kurucu, and E. Das, *J. Mater. Sci. Mater. Electron.* 31, 12715 (2020).
24. M. Simon, *Sze, Physics of Semiconductor Devices*, 2nd ed., (Hoboken: Wiley, 1979).

25. A. Karabulut, H. Efeoglu, and A. Turut, *J. Semicond.* 38, 054003 (2017).
26. A. Türüt, *Turkish J. Phys.* 44, 302 (2020).
27. L.B. Tasyurek, M. Sevim, Z. Caldiran, S. Aydogan, and O. Metin, *Mater. Res. Express* 5, 015060 (2018).
28. S. Altindal, S. Karadeniz, N. Tugluoglu, and A. Tataroglu, *Solid. State. Electron.* 47, 1847 (2003).
29. O. Ongun, E. Tasci, M. Emrullahoglu, U. Akin, N. Tugluoglu, and S. Eymur, *J. Mater. Sci.: Mater. Electron.* 32, 15707 (2021).
30. D.E. Yıldız, S. Karadeniz, and H.H. Gullu, *J. Mater. Sci. Mater. Electron.* 32, 20130 (2021).
31. H. Patel, K. Patel, A. Patel, H. Jagani, K.D. Patel, G.K. Solanki, and V.M. Pathak, *J. Electron. Mater.* 50, 5217 (2021).
32. S. Altındal, O. Sevgili, and Y. Azizian-Kalandaragh, *IEEE Trans. Electron Devices* 66, 3103 (2019).
33. N. Tugluoglu, S. Karadeniz, and S. Altındal, *Appl. Surf. Sci.* 239, 481 (2005).
34. S.M. Sze, *Physics of Semiconductor Devices*, 2nd ed., (Hoboken: A Wiley-Interscience Publication, 1981).
35. H. Norde, *J. Appl. Phys.* 50, 5052 (1979).
36. E.H. Rhoderick, and R.H. Williams, *Metal-Semiconductor Contacts* (Oxford: Clarendon Press, 1988).
37. S.K. Cheung, and N.W. Cheung, *Appl. Phys. Lett.* 49, 85 (1986).
38. S. Karatas, S. Altindal, A. Turut, and A. Ozmen, *Appl. Surf. Sci.* 217, 250 (2003).
39. L.D. Rao, and V.R. Reddy, *AIP Conf. Proc.* 120020, 120020 (2016).
40. S. Karatas, N. Yildirim, and A. Turut, *Superlattices Microstruct.* 64, 483 (2013).
41. I. Missoum, Y.S. Ocak, M. Benhaliliba, C.E. Benouis, and A. Chaker, *Synth. Met.* 214, 76 (2016).
42. A. Kocyigit, I. Orak, Z. Caldıran, and A. Turut, *J. Mater. Sci. Mater. Electron.* 28, 17177 (2017).
43. A. Turut, M. Coskun, F.M. Coskun, O. Polat, Z. Durmus, M. Caglar, and H. Efeoglu, *J. Alloys Compd.* 782, 566 (2019).
44. S. Karatas, *Microelectron. Eng.* 87, 1935 (2010).
45. C. Bilkan, S. Altındal, and Y. Azizian-Kalandaragh, *Phys. B Condens. Matter* 515, 28 (2017).
46. Z. Caldıran, *J. Alloys Compd.* 816, 152601 (2020).
47. O. Sevgili, Y. Azizian-Kalandaragh, and S. Altındal, *Phys. B Condens. Matter* 587, 412122 (2020).

Publisher's Note Springer Nature remains neutral with regard to jurisdictional claims in published maps and institutional affiliations.